

Article

Low Frequency Waves Detected in a Large Wave Flume under Irregular Waves with Different Grouping Factor and Combination of Regular Waves

Luigia Riefolo ¹ , Pasquale Contestabile ^{2,*}, Fabio Dentale ³ and Guido Benassai ⁴ 

¹ Department of Civil and Environmental Engineering DICA, Politecnico di Milano, 20133 Milan, Italy; luigia.riefolo@polimi.it

² Department of Engineering, University of Campania “Luigi Vanvitelli”, 81031 Aversa, Italy

³ MEDUS (Maritime Engineering Division University of Salerno) Department of Civil Engineering, University of Salerno, 84084 Fisciano (SA), Italy; fdentale@unisa.it

⁴ Department of Engineering, Parthenope University of Naples, 80133 Naples, Italy; guido.benassai@uniparthenope.it

* Correspondence: pasquale.contestabile@unicampania.it; Tel.: +39-081-501-0245

Received: 26 January 2018; Accepted: 19 February 2018; Published: 23 February 2018

Abstract: This paper describes a set of experiments undertaken at Universitat Politècnica de Catalunya in the large wave flume of the Maritime Engineering Laboratory. The purpose of this study is to highlight the effects of wave grouping and long-wave short-wave combinations regimes on low frequency generations. An eigen-value decomposition has been performed to discriminate low frequencies. In particular, measured eigen modes, determined through the spectral analysis, have been compared with calculated modes by means of eigen analysis. The low frequencies detection appears to confirm the dependence on groupiness of the modal amplitudes generated in the wave flume. Some evidence of the influence of low frequency waves on runup and transport patterns are shown. In particular, the generation and evolution of secondary bedforms are consistent with energy transferred between the standing wave modes.

Keywords: spectral analysis; low frequency; wave grouping; eigen analysis; eigenmode; random waves; combination waves

1. Introduction

Extreme storms may significantly affect the coastal environment, especially in terms of erosion and sediment transport. They can provoke disastrous consequences such as sediment transport beyond the surf zone to unusual depths [1]. Waves reaching a coastline release the majority of their energy and momentum within the surf zone as intense turbulence generated at the front face of the breaker. However, a portion of that energy is transferred to low frequency modes [2], like Low Frequency Waves, longshore currents, rip-currents and shear waves, that are oscillations generated by a shear instability of the mean longshore current profile, especially on barred beaches [3,4]. Low-frequency waves can be generated from intense interaction between short waves and between short waves and long waves at the surf-swash boundary [5,6].

Cross-shore standing long wave swash oscillations are usually forced by infragravity frequency ($f < 0.05$ Hz) waves [7–14] as are swash oscillations due to waves traveling or oscillating along the water edge, parallel to the mean-water line (edge waves) [15–19]. Although wind-waves or short-waves (typical frequency of about 0.1 Hz) are the major force behind the swash zone (SZ) dynamics, the importance of the SZ for the generation/transformation of low frequency motions has been recognized [6,20–23]. In the SZ, in fact, while the final dissipation of short-wave (wind and

swell) energy occurs, the Low Frequency Wave (LFW hereinafter) energy (typical wave frequencies between 0.03 and 0.003 Hz) is, generally, reflected back seaward. In addition, intense interaction between short waves and between short waves and long waves at the surf-swash boundary can lead to the generation and reflection of further LFW [5,6]. Superficial SZ hydrodynamics, subsurface SZ hydrodynamics, sediment dynamics and co-related beachface morphodynamics determine and are strongly determined by the frequency of swash motion in no-tidal seas [24–31]. Nonlinearity is a major mechanism responsible for LFW. However, amplitude modulation of waves surface elevation (also termed wave grouping or groupiness) represents another predominant feature in short wave processes affecting long wave generation.

The Groupiness Factor (GF) is a measure of the degree of grouping or rather than of the amplitude modulation of the incident wave field. It is defined as the standard deviation of Smoothed Instantaneous Wave Energy History (SIWEH) normalized with respect to its mean value. A technique which involves no low-pass filtering to compute the low frequency part of the square of the water surface elevation is the Hilbert transform technique. Groupiness Factor is a global measure of the variance contained, in the entire low frequency, part of the square of the water surface elevation [32,33].

Some questions still remain as to which mechanisms dominate under different surf zone conditions. For example, while it is well known that more regular waves (swell waves) tend to promote recovery but irregular waves (sea waves) tend to promote erosion, it is not clear if this is related to changes in nonlinearity or groupiness or to changes in energy [34–36].

In this context, the project SUSCO (Swash zone response under grouping Storm Conditions) used the Hydralab III facility at the large wave flume of the Maritime Engineering Laboratory (LIM), Catalonia University of Technology (UPC) [37]. The objectives of the project were to compare the shoreline response and the SZ hydrodynamics of various wave regimes. In particular, the beach response between monochromatic conditions and wave groups were investigated as a direct result of the wave groupiness. The effects of forced and free long waves induced by the groupiness were also examined.

The data provided by the SUSCO campaign represent a comprehensive and controlled series of tests for evaluating in detail many complex phenomena affecting the hydro-morphodynamic in the surf and SZ. Starting from that dataset, the main aim of this study is to compare the effect of various wave regimes on very low frequencies generations. In particular, wave flume seiche is investigated as a potential effect of low-frequency energy during the experiments. As known, wave generation in an enclosed flume could cause seiche owing to wave reflections or wave grouping effects that can transfer wave energy to low-frequencies [38].

Often wave flume experiments involve wave reflection generated by structure/beaches. Nowadays this problem is solved by controlling the paddle through an active reflection system, which is not applicable to long wave absorption. When active absorption is applied, the reflected waves approaching the generator are predicted in real time and paddle control signals are modified to absorb the waves approaching the generator. The result is that the control of the incident waves is maintained throughout the test. The wave resonance in the wave flume is generated by the reflection phenomena occurring when the wave frequency begins to be equal to the fundamental or harmonic resonant frequency of the flume. Lengthwise oscillations of long waves in a flume can be troublesome as they take a long time to dissipate, owing to their high reflectivity [39].

The wave generator does not have the capability to absorb long wave energy, it is first necessary to see if any of the long wave activity is due to resonance of certain frequencies with the wave flume (seiche). The natural frequencies of the wave flume have to be determined by eigenvalue analysis.

Bellotti et al. [40], on the basis of data from tests performed at the same large wave flume of LIM, found a non-negligible low-frequency component that can be addressed to seiches of the flume. Resonant seiche response in a wave flume (or wave tank) represents an unfortunate drawback, especially for mobile bed experiments. In a resonant condition, the excitation of low-frequency (resonant) modes of the wave flume results in components whose amplitudes can increase to be of the

same order as the primary waves [41]. Some authors are concerned about resonant cross-tank seiching that would occur in a wave flume under different wave conditions [42,43]. The variation in seiching has been found to modify the final equilibrium profile and the bar-trough morphology [35,36].

For these reasons, it is important to quantify any influence of the low-frequency for erosive and accretive wave conditions especially concerning the interpretation of different hydro-morphodynamic effects. Furthermore, among the generated waves of the experimental tests described in the Section 2, the results for random and combination tests are presented here.

Low frequencies are studied through the Spectral and Eigen analysis as presented in Section 3, estimating the frequency of the dominant seiches in the wave flume. Furthermore, the influence of the low frequencies on the wave energy spectra is investigated using a numerical solution, which adopts as input the measured data of the beach profiles of the case studies. Finally, combined analysis between modes for surface displacement and net sediment transport has been used to clarify the influence of LFW on morphodynamics. The results of these analyses are shown in Sections 4 and 5; then the main findings are summarized in Section 6.

2. Experimental Setup

In this paper, wave interaction with a rubble mound breakwater has been modeled using numerical simulations. The CIEM (Canal d'Investigació i Experimentació Marítima) large-scale wave flume is 100 m long, 3 m wide and up to 4.5 m deep. The beach consisted of commercial well-sorted sand with a medium sediment size (d_{50}) of 0.25 mm, with a narrow grain size distribution ($d_{10} = 0.154$ mm and $d_{90} = 0.372$ mm) and a measured settling velocity (w_s) of 0.034 m/s. The experimental profile and equipment distribution is presented in Figure 1. The x-coordinate origin is at the wave paddle at rest condition before starting the waves and positive toward the shoreline. The movable bed profile started after 31 m of concrete with a section 1:20 slope from $x = 31$ to 37 m prior to a plane bed, from $x = 37$ to 42 m, followed by a 1:15 slope plane beach (Figure 1). Prior to running each wave condition, the water depth was performed by manual reshaping and then compacted by running 10 minutes of 'smoothing' wave conditions, in order to return almost the same initial profile. The water depth at the toe of the wedge-type wave paddle was 2.5 m [44].

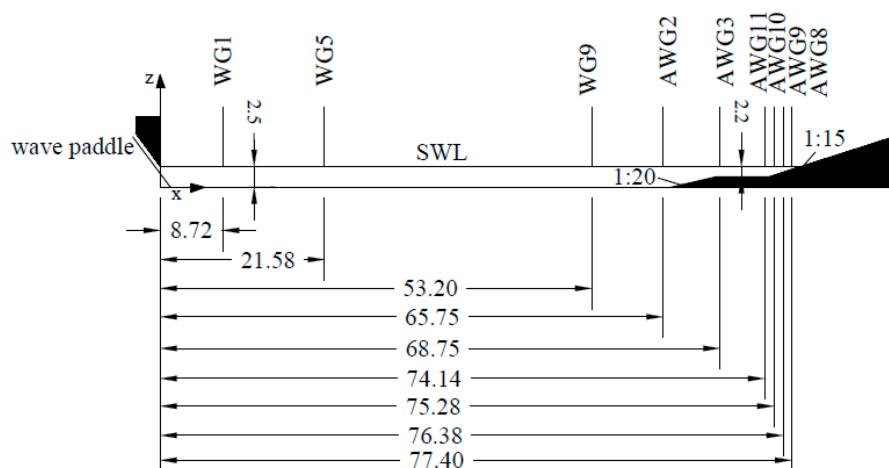


Figure 1. Longitudinal cross-section of the Catalonia University of Technology (UPC) flume and detail of acoustic wave gauges and wave gauges location (length in m).

Among all the instruments installed and used in the controlled area [45], 6 Acoustic Wave Gauges (AWGs), 10 Resistant Wave Gauges (WGs), and 1 beach profiler were acquired. These instruments were sampled at 20 Hz according to the characteristics of the acquisition system (Figure 1).

The bottom profile information was acquired by means of a mechanical bed profiler that measures the emerged and submerged profile along a central line of the flume. The mechanical profiler consists

of a wheel at the end of a pivoting arm which is mounted on a moving platform along the flume. A computer records the velocity of the platform and the angle rotation of the arm. Those data are used to extract the X and Z flume bathymetry. The overall vertical profile accuracy is therefore estimated to be ± 10 mm. Such accuracy is comparable with more recent experimental study on beach profile evolution [46], where the standard deviation of the vertical profile was found to be equal to 0.1 cm and 0.2 cm for the emerged and submerged beach profile, respectively. The vertical datum for the profile data is the sea water level (SWL in Figure 1). The horizontal datum is that of the reference point in the flume, which is 7.4 m from the wavemaker and approximately 36 m seaward of the beach toe.

As previously mentioned, the tests were carried out for two different levels of energy flux, defined as “erosive” and “accretive”, covering a broad range of wave amplitudes, short and long wave frequencies, modulation rates and group frequencies. The behavior of the two wave regimes was forecasted by mean of the dimensionless sediment fall velocity number (Dean number) [47] and on the basis of previous experiments in the CIEM flume using similar wave conditions. The final profiles and net sediment transport are consistent with these initial estimates. Therefore, hereinafter “erosive test” and “accretive test” refer to wave conditions able to produce morphological patterns (over the whole beach profile) in which erosive or accretive conditions dominate, respectively. The following waves were appointed:

- random waves with different Grouping Factors (GF);
- combination of free partial standing long waves plus monochromatic short waves (hereinafter, combined waves);
- regular monochromatic;
- bichromatic waves (including bound long waves).

Among all the tests generated during the test campaign, random and combination waves in both cases erosive and accretive are here examined. In the Tables 1 and 2 the wave characteristics such as wave height H (m), related to the different wave components, and wave period T (s) for those tests in erosive and accretive conditions are listed. Considering the measured sediment fall velocity of 0.034 m/s, the beach was morphologically characterized by intermediate and reflective conditions for erosive and accretive waves regimes respectively [48]. According to Wright and Short [49], the beach state is a function of breaker height, period and of the sediment size.

Table 1. Wave characteristics for accretive conditions.

Test	H (m)	T (s)	Wave Type
CA_1	0.226	6	Combination
	0.038	30	
CA_2	0.226	6	Combination
	0.038	15	
RA_1	0.319	6.7	Random GF = 0.96
RA_2	0.319	6.7	Random GF = 1.08

Four random wave trains, RE_1, RE_2, RA_1, RA_2, were generated with the same variance based on wave height and the same peak frequency as their corresponding monochromatic pair. On the other hand, to generate long-wave short-wave combinations, the monochromatic conditions have been perturbed by small amplitude long waves, added to the control signal. Hence, cases CE_1, CE_2, CA_1, and CA_2 represent the addition of free long waves to otherwise monochromatic wave conditions (Tables 1 and 2). Controlled wave generation was achieved by a wedge-type wave paddle, particularly suited for intermediate-depth waves. The wave generation software used for controlling the wave paddles was AWASYS5 [50].

Table 2. Wave characteristics for erosive conditions.

Test	H (m)	T (s)	Wave Type
CE_1	0.370	3.7	Combination
	0.038	30	
CE_2	0.370	3.7	Combination
	0.038	15	
RE_1	0.530	4.1	Random GF = 1
RE_2	0.530	4.1	Random GF = 1.1

The groupiness was slightly varied as well as the phases, obtaining random waves of identical energy spectrum (conforming to JONSWAP spectrum with $\gamma = 3.3$) [48]. The Grouping Factor, which measures the degree of grouping, or rather than of the amplitude modulation of the incident wave field, is computed according with Hald [51] (Equation (1)) as the standard deviation σ of half the squared wave surface elevation envelope curve $E(t)$ relative to the squared variance σ^2 of the surface elevation $\eta(t)$ as follows:

$$GF = \frac{\sigma[E(t)]}{\sigma^2[\eta(t)]} \quad (1)$$

In particular, the half squared envelope signal is computed by the Hilbert transformation. The standard approach of wave generation is to use random uncorrelated phases which in the average leads to $GF = 1.0$ along with $\sigma^2 \approx 0.13$ for 500 waves. [48–51]. Greater values of GF suggest that small waves tend to be succeeded by small waves, and large waves by other large waves.

All tests started from a similar initial 1/15 handmade slope. For the erosive conditions the reshaping took place along the active profile, while the reshaping occurred from the landward edge of the bar trough to the run-up limit on the accretive conditions. The tests were composed of four steps which included five bottom profiles. Each test lasted 24 min and was repeated 6 times. Consequently, the final profile (P4) was generated after a total active wave time equal to 144 min.

Different bottom profiles were acquired during each wave testing condition. One at the beginning of the experiments (P0), and consecutively at the end of the 1st (P1), 2nd (P2), 4th (P3) and 6th (P4) runs for each of the 13 wave conditions.

Tests were a compromise between the desire to reach an equilibrium profile and the available experimental time.

3. Methods

Data treated in this work concern the first step of 24 min duration for each test. The wave conditions started with a similar initial beach profile for both wave conditions, accretive and erosive, respectively, as shown in Figures 2 and 3. For this reason, the results discussed below can be considered without significant influence from morphodynamic feedback during the measurements. Such conditions afford to obtain reliable observations of hydrodynamic behaviors of LFW also in movable bed experiments.

Furthermore, before carrying out the computation of net sediment volume variation ΔV_{SZ} , bed elevation data have been corrected. In fact, it is worth mentioning that the total beach volume of each profile was not the same. Due to profiler measurement errors, in particular the inability to accurately measure ripple volumes and some non-uniformity of the profile, calculation of ΔV along the whole profile never returns identically zero. Therefore, errors in the calculated ΔV were corrected by distributing the mismatch in sediment volume along the whole profile, leading to a zero value of ΔV . Generally, the error distributed is of a few millimeters, hence the correction does not significantly affect the volume computation. This approach derives from the method proposed by and Baldock et al. [18] for calculation of the net time-averaged sediment transport. The analysis assumed a depth of closure for the sediment transport calculations at $x = 60$ m (at a water depth of approximately 1 m), and

applied the sediment continuity correction over the active profile, that is, landward of $x = 60$ m or shallower than 1 m. This enables greater resolution and improved accuracy in the ΔV calculations. Closure errors corresponded to a mean error in vertical elevation across the profile that ranged from 3 mm to 15 mm, with an average of 9 mm over all tests, which is consistent with the estimated accuracy of the bed profiler. However, other methodologies could be applied to reconstruct transverse profiles and to study coastal evolution, in particular performing a comparison of aerial photographs according to Muñoz-Pérez et al. [52].

In the present paper, two kinds of analysis have been carried out, as described in the following two sub-sections.

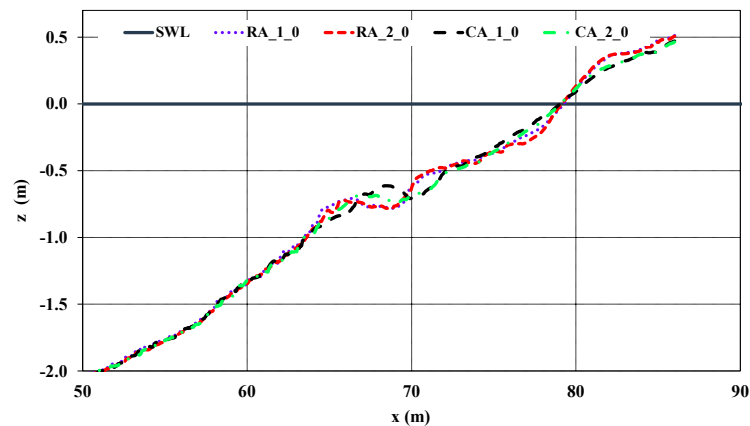


Figure 2. Initial beach profiles of the accretive tests, random and combination, respectively.

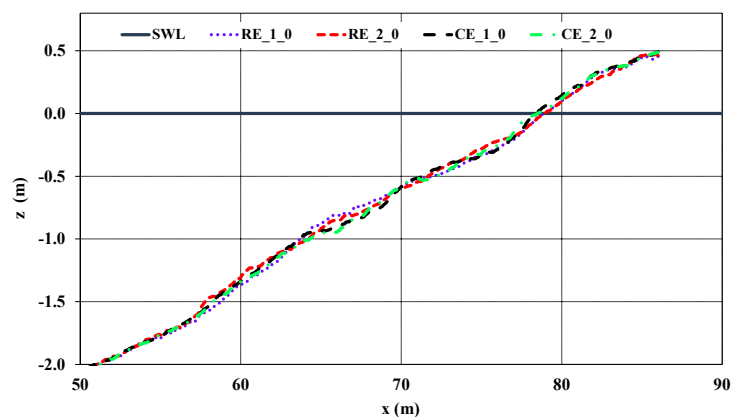


Figure 3. Initial beach profiles of the erosive tests, random and combination, respectively.

3.1. Spectral Analysis

On the basis of the time series of surface elevations the spectral analysis has been performed to evaluate the energy characteristics induced by wave motion. The response of low frequency variations in the large wave flume for random and combination tests has been analyzed. In addition, the spectra response is observed taking into account the time series of the water surface elevation in accretive and erosive wave conditions.

According to Molloy [53], the spectral density represents the momentum corresponding to the specific frequencies. A higher momentum or spectral density corresponds to a larger amplitude oscillation.

Operatively, a Fast Fourier Transform (FFT) is applied to execute spectral analysis for each test. Once the peaks in the spectra corresponding to low-frequencies and harmonics are identified, they are later compared with wave modes determined by the Eigen analysis, as described in the following.

3.2. Eigen Analysis

It is first necessary to study if any of the long wave activity is due to resonance of specific frequencies with the wave flume (hereinafter “seiche”). According to Rabinovich [54] the resonance occurs when the dominant frequencies of the external forcing match the Eigen frequencies of the flume.

In particular, seiche is long-period standing oscillation in an enclosed basin. The resonant (eigen) frequency of seiche is determined by basin geometry and water depth. The set of eigen frequencies and associated modes are a fundamental property of a specific basin [54]. The mode of a seiche is the number of nodes it has within the system. The period of a seiche with “ n ” nodes is given by Merian’s formula [55]. This assumes that the basin is rectangular, with a uniform depth. The related period can be computed as:

$$T_n = \frac{2L}{n\sqrt{gh}} \quad (2)$$

where: T_n is the period of an n th mode seiche; L is the wavelength of the seiche (length of the basin); n is the number of nodes/modes of the seiche; g is the acceleration due to gravity 9.81 m/s^2 , and h is the average water depth.

The period derived from Equation (2) is the time it takes for the waveform to oscillate from one end of the basin to the other and back. That is, to travel a distance of twice the basin length. Obviously, the different seiche modes are not mutually exclusive. Seiches with various different modes can occur together in a system. However, the fundamental oscillation is usually dominant, as first shown by Wilson [56].

In the next section the results of the calculated Eigenvalues and Eigenmodes through a numerical approach are shown. This method was presented by Kirby et al. [57] to determine the family of Eigenmodes for measured wave flume geometry. The resulting matrix eigenvalue problem, derived from the next equation (Equation (3)), is solved using the EIG routine in MATLAB™.

$$q_{xx} - \lambda z^{-1}q = 0 \quad (3)$$

where $q = zu$ is the volume flux, u the horizontal velocity, z the water depth, $\lambda = \omega^2/g$ represents the Eigenvalue for the problem and ω the angular frequency. Equation (3) is finite differenced using centered second-order derivatives. The corresponding expansion, orthogonality condition, and dispersion relation are given by:

$$q(x) = \sum_{n=1}^{\infty} q_n F_n(x) \quad (4)$$

$$\int_0^L z^{-1} F_n F_m dx = 0; \quad n \neq m \quad (5)$$

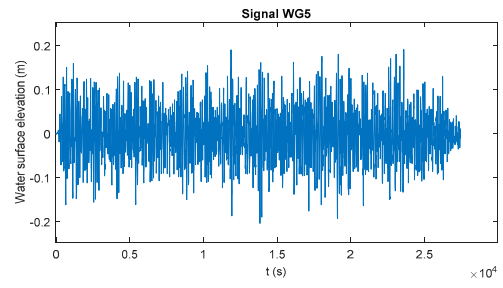
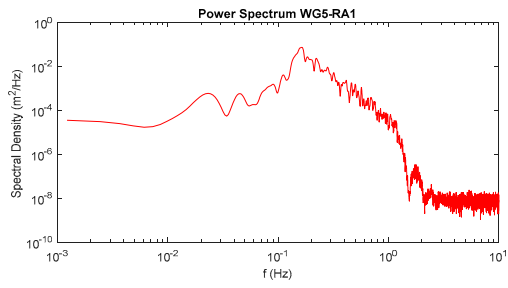
$$\omega_n^2 = -g \frac{\int_0^L (F_n')^2 dx}{\int_0^L z^{-1} F_n^2 dx} \quad (6)$$

in which F_n and F_m represent the family of eigenmodes of order n and m respectively.

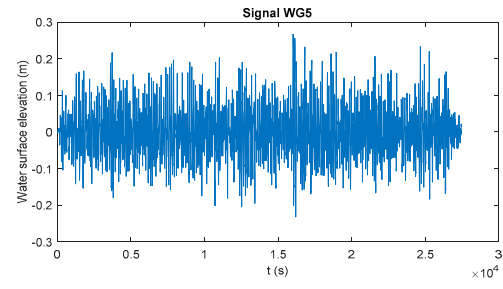
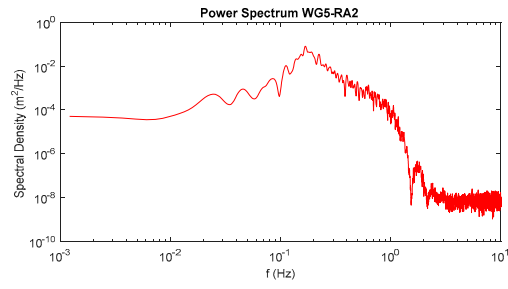
In this study, the four families of eigenmodes, F_1 , F_2 , F_3 and F_4 , have been determined by solving numerically Equations (3)–(6).

4. Results and Discussion

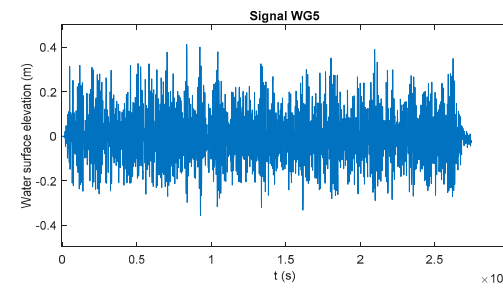
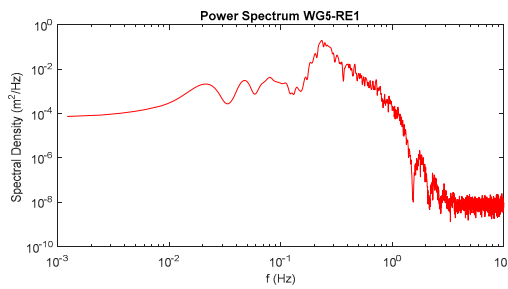
Spectral power density (expressed in m^2/Hz) and water surface elevation signal plots (related to the wage gauge WG5 at 21.58 m in the wave flume) are presented in Figure 4.



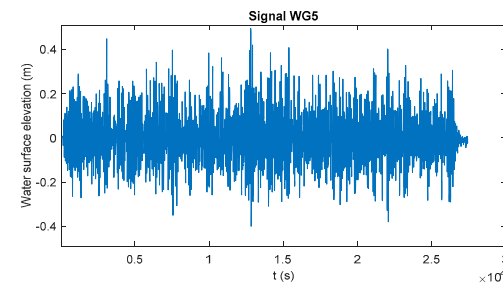
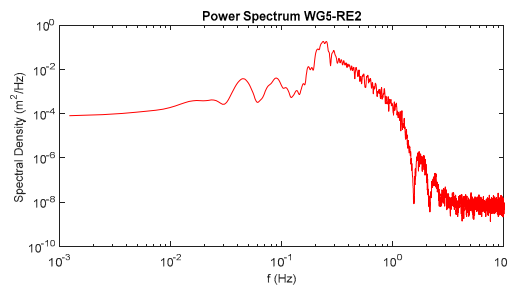
(a)



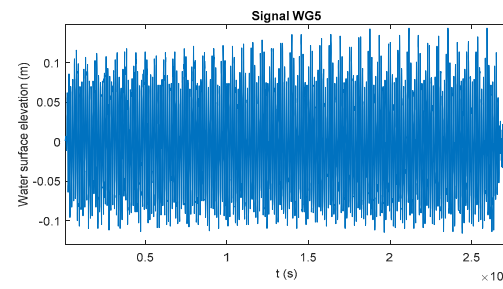
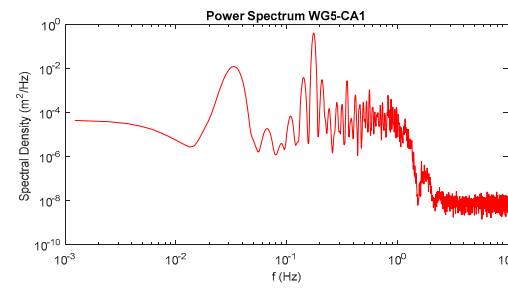
(b)



(c)



(d)



(e)

Figure 4. Cont.

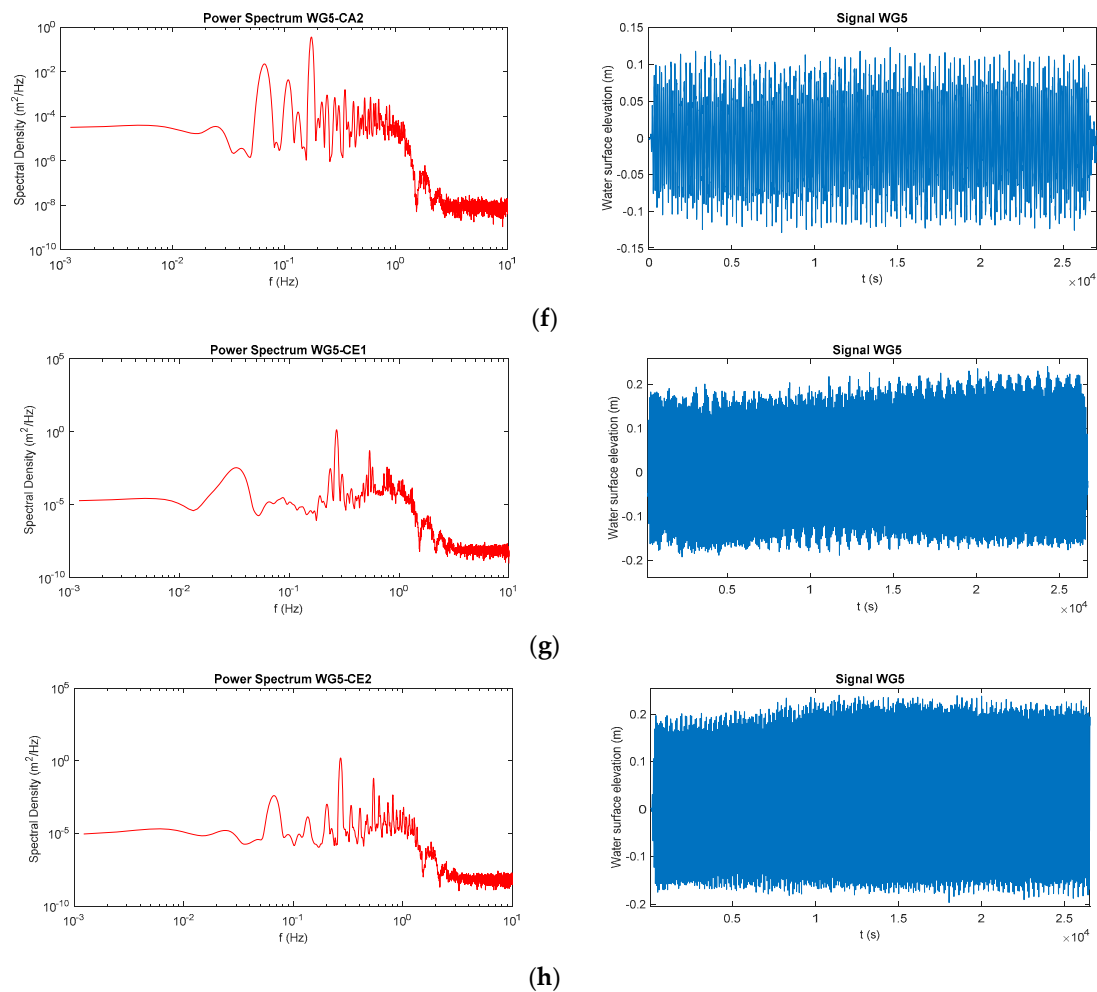


Figure 4. Power spectral density and Time series water surface elevation for test: (a) RA_1 (GF = 0.96); (b) RA_2 (GF = 1.08); (c) RE_1 (GF = 1); (d) RE_2 (GF = 1.1); (e) CA_1; (f) CA_2; (g) CE_1 and (h) CE_2.

It is possible to note the great variability of the oscillation modes even in the region of low frequencies, according to Cáceres and Alsina [58]. In fact, the authors found that random waves need longer time periods to reach a stationary position. These are wave conditions with wider breaking areas. Furthermore, they found that the wave group and short wave period ratio plays a significant role in the suspended sediment fluxes through the generation of harmonics with longer periods than the wave group. This is due to the fact that the time evolution of morphological features is affected by the length of the breaking area.

Focusing on frequencies under 0.1 Hz, the power spectral density peak values and the corresponding frequencies for random tests in both the erosive and accretive case are reported in Tables 3 and 4. Those values are related to the first, second and third harmonic. Water surface elevation time series are between -0.2 and 0.2 m meanly for all the studied tests.

Furthermore, it is noted that increasing the grouping factor the spectral density associated to the 1st harmonic strongly decrease in random waves. In fact, for cases RA_2 and RE_2 the lowest frequency peak is relatively less pronounced (Tables 3 and 4). That energy density is moved in the higher part of the spectra, as further demonstrated by Table 5, where power levels associated with various sections of the spectra are reported. In particular, for erosive tests, no relevant difference in the 2nd and 3rd harmonic energy density is observed. Moreover, beyond the first harmonic, a monotone trend in wave spectra is found, while for accretive conditions the spectral density slightly increases moving toward lower frequencies. It is notable as for tests RE_1 and RE_2 the third harmonic represents the

highest peak before the carrier wave (frequency of about 0.25 Hz). For accretive conditions a slight peak appears at about 0.11 Hz.

Table 3. Peak frequencies, periods and power spectral density for RA_1 and RA_2 tests.

	Harmonics	f (Hz)	T(s)	E (m ² /Hz)
Test RA_1	1st harmonic	0.02319336	43.1157895	0.00059542
	2nd harmonic	0.04516602	22.1405405	0.00058067
	3rd harmonic	0.09033203	11.0702703	0.00155648
Test RA_2	1st harmonic	0.02441406	40.9600042	0.00052997
	2nd harmonic	0.04516602	22.1405405	0.00089923
	3rd harmonic	0.08544922	11.7028571	0.00267999

Table 4. Peak frequencies, periods and power spectral density for RE_1 and RE_2 tests.

	Harmonics	f (Hz)	T(s)	E (m ² /Hz)
Test RE_1	1st harmonic	0.02197266	45.5111111	0.00211399
	2nd harmonic	0.04760742	21.0051282	0.00310199
	3rd harmonic	0.08056641	12.4121212	0.00424879
Test RE_2	1st harmonic	0.02319336	43.1157895	0.00041757
	2nd harmonic	0.04516602	22.1405405	0.0038171
	3rd harmonic	0.08911133	11.2219178	0.0040941

Table 5. Power spectral density for various sections of the spectra for the random tests.

E (m ² /Hz)	RE_1	RE_2	RA_1	RA_2
total	1.22×10^1	1.20×10^1	3.37×10^0	4.00×10^0
<0.1 Hz	1.45×10^{-1}	1.19×10^{-1}	3.97×10^{-2}	6.34×10^{-2}
<0.03 Hz	2.18×10^{-2}	6.68×10^{-3}	5.26×10^{-3}	5.07×10^{-3}

In the case of combination waves the 1st harmonic does not decrease strongly, as for the combination cases, but at about 0.8 Hz. Moreover, a power spectral response corresponding to twice the wave frequency is noted, especially for the erosive wave regimes (Figure 4e–h). In Tables 6–8 the peak frequencies, periods and power spectral density are summarized, also related to various sections of the spectra. In particular, the difference for the combination waves in accretive and erosive conditions is higher when is considered the power spectral density at frequencies less than 0.03 Hz.

Table 6. Peak frequencies, periods and power spectral density for CA_1 and CA_2 tests.

	Harmonics	f (Hz)	T(s)	E (m ² /Hz)
Test CA_1	1st harmonic	0.032958984	30.34074074	0.01233396
	2nd harmonic	0.065917969	15.17037037	0.00001770
	3rd harmonic	0.108642578	9.20449438	0.00004718
Test CA_2	1st harmonic	0.025634766	39.00952381	0.00002758
	2nd harmonic	0.041503906	24.09411765	0.00000737
	3rd harmonic	0.067138672	14.89454545	0.02348628

For tests RA_1 and RA_2 a sort of spreading around the carrier wave should be noted (frequency of about 0.158 Hz and 0.167 Hz respectively). In particular, this spreading takes the form of a second downshifted peak, more evident for RA_2. The shift from the main wave is of about ± 0.045 Hz, that is, an amount approximately equal to the second harmonic. It is worth noting that the presence of 2nd harmonic disturbance on the carrier wave is also perceptible for RE_2. The latter turns out to

be important looking at Figure 5, where spectral density ratio between third and second mode and between second and first harmonic are summarized. A heuristic explanation for the singular behavior of RE_2 and the influence of the second harmonic could be addressed to the enhanced non-linear interactions due to wave groupiness forcing a long wave at the frequency of second harmonic. In this vein, it is worth considering that the largest wave height (both maximum and significant) compared to others wave conditions with the same energy flux is formed precisely during RE_2. And just like the undertow largely follows the instantaneous wave height [59], the larger waves in the groups could dominate the whole hydrodynamics.

Table 7. Peak frequencies and power spectral density for CE_1 and CE_2 tests.

	Harmonics	f (Hz)	T(s)	E (m ² /Hz)
Test CE_1	1st harmonic	0.03295898	30.34074074	0.00314475
	2nd harmonic	0.06713867	14.89454545	0.00000949
	3rd harmonic	0.10805664	12.41212121	0.00002413
Test CE_2	1st harmonic	0.023193359	43.11578947	0.00000319
	2nd harmonic	0.040283203	24.82424242	0.00000234
	3rd harmonic	0.067138672	14.89454545	0.00393993

Table 8. Power spectral density for various sections of the spectra for the combination tests.

E (m ² /Hz)	CE_1	CE_2	CA_1	CA_2
total	1.11×10^1	1.32×10^1	3.43×10^0	3.17×10^0
<0.1 Hz	2.53×10^{-2}	3.14×10^{-2}	9.80×10^{-2}	1.86×10^{-1}
<0.03 Hz	4.50×10^{-3}	1.35×10^{-4}	1.81×10^{-2}	3.83×10^{-4}

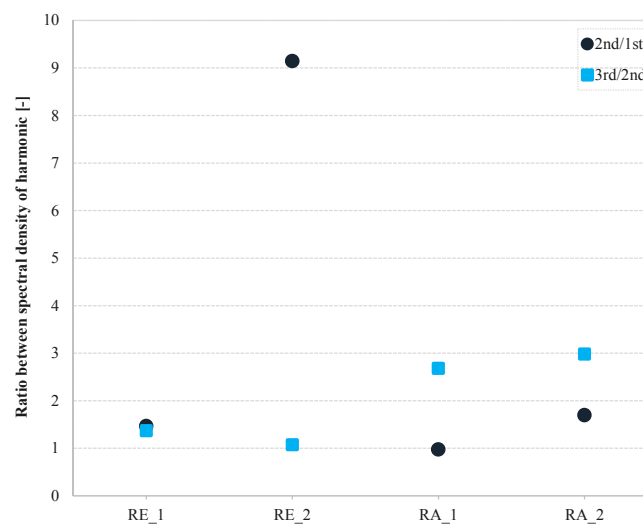


Figure 5. Ratio between spectral density level at different harmonics of the random tests.

The ratios between spectral density level at different harmonics of the combination tests show a similar behavior in the cases of erosive and accretive regime for the monochromatic waves perturbed with larger (CE_1 and CA_1) and smaller (CE_2 and CA_2) long waves, respectively (Figure 6).

In order to clarify the origin of these waves, the frequencies of the longest standing waves in the flume have been evaluated and compared with the measured lowest frequencies. The natural frequencies of the wave flume are determined by Eigenvalue analysis. The calculated periods and frequencies using formulas found in the literature were published in recent research conducted by Riefolo et al. [60]. Measured and numerically predicted mode periods are compared in Figures 7 and 8,

where a linear deviation from the bisector line is highlighted (see black dashed line). The frequencies calculated with the formula proposed by Merian [55] are shown in Table 9. Appreciably, correlation between the measured and calculated frequencies has been found. These tests, in fact, show a good correspondence between the calculated and measured frequencies especially for the first and second harmonic, for which the influence of wave flume-generated seiching can be definitively highlighted in the case of random waves (Figure 7). On the other hand, the monochromatic wave perturbed with the larger long waves for the erosive condition (CE_1) gives different variation, in the measured and calculated Eigenmodes, of the case in the accretive conditions (CA_1). Instead, a similar variation of the measured and calculated Eigenmodes for the tests CA_2 and CE_2 is highlighted where the monochromatic wave was perturbed with smaller long waves, for both analyzed conditions, accretive and erosive, respectively (Figure 8). This similarity has been confirmed by the ratios between spectral density level at different harmonics of the combination tests, as previously described in Figure 6.

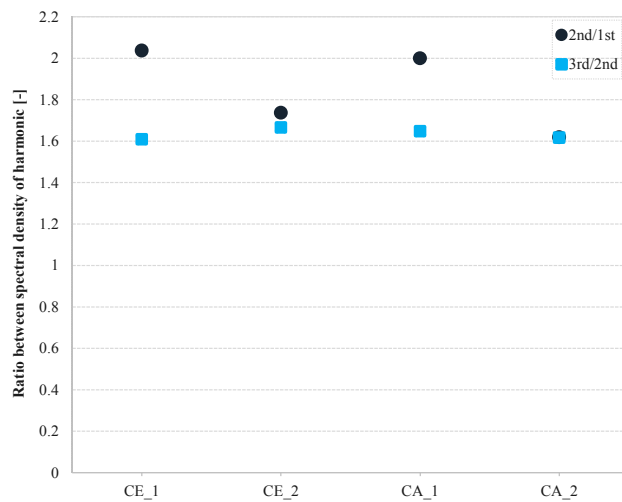


Figure 6. Ratio between spectral density level at different harmonics of the combination tests.

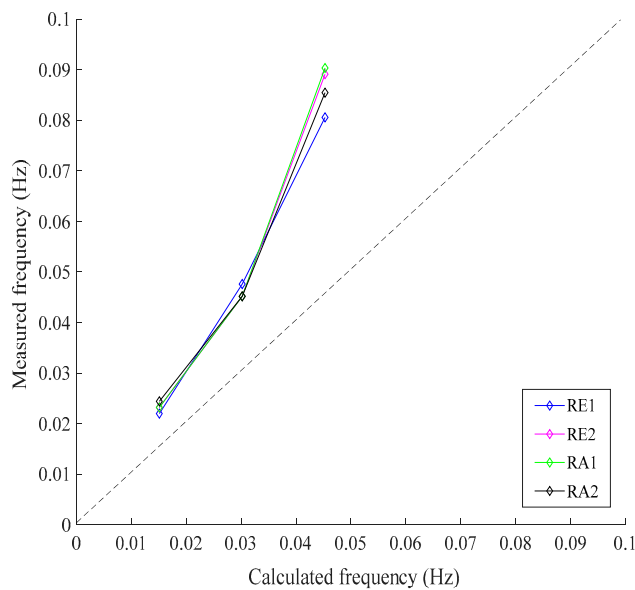


Figure 7. Frequencies plot of measured versus calculated Eigenmodes with formula for rectangular basin for random tests in the case of accretive and erosive condition.

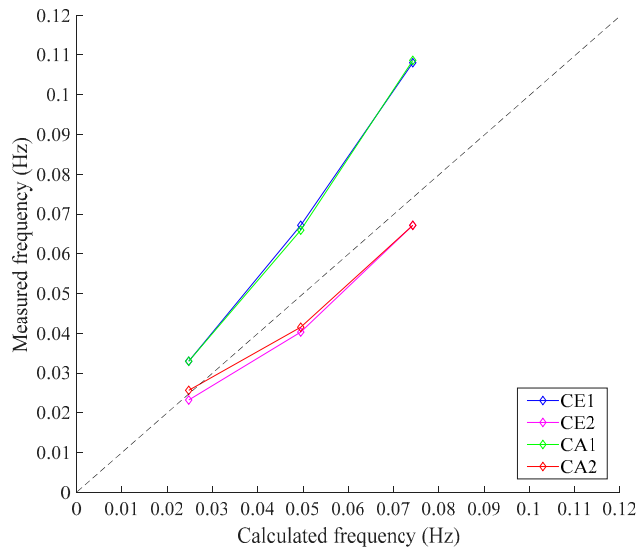


Figure 8. Frequencies plot of measured versus calculated Eigenmodes with formula for rectangular basin for combination tests in the case of accretive and erosive condition.

Table 9. Eigen values calculated through the formula proposed by Merian [55].

Mode	f (Hz)
1st	0.02474874
2nd	0.04949747
3rd	0.07424621

5. Additional Considerations

The effects of the LFWs have been assessed by a set of the four lowest computed modes (F_1 – F_4) for volume flux in the wave flume, shown in Figures 9 and 10. Mode periods are computed by the eigen analysis based on water depth z . Very interesting results can be identified:

- A strong non-linear pattern of F_1 – F_4 is identified for all the tests in proximity of breaking zone;
- Clear opposite behaviours of volume flux eigenmodes are shown for accretive and erosive wave conditions in the case of random and combination waves, except for the test CE_2;
- A different variation of the Eigenmodes for the combination tests in the erosive, clearly, due to the non-linearity effects;
- The monochromatic wave perturbed with the larger long waves for the erosive condition (CE_1) has an opposite variation of the Eigenmodes, than the monochromatic wave perturbed with smaller long waves (CE_2).

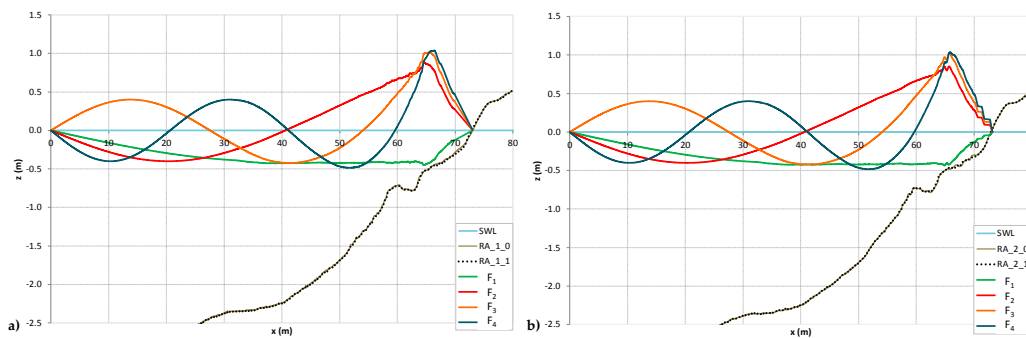


Figure 9. Cont.

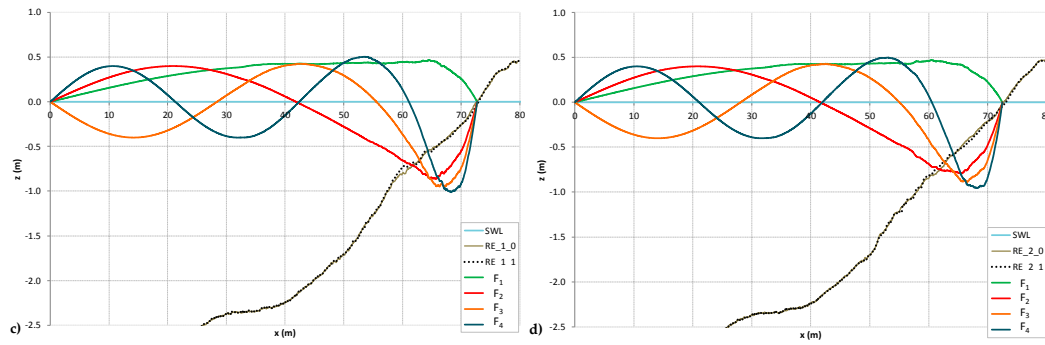


Figure 9. Eigenmodes for volume flux q related to the profile measured in random test: (a) RA_1; (b) RA_2; (c) RE_1 and (d) RE_2.

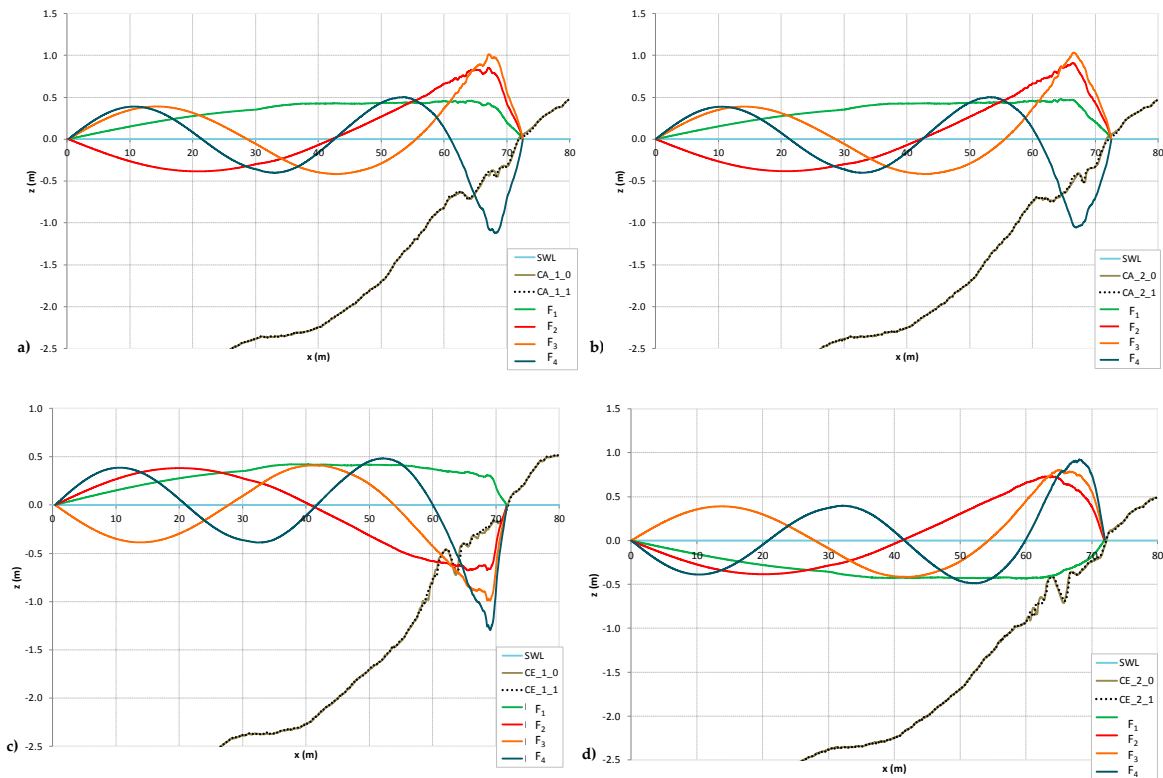


Figure 10. Eigenmodes for volume flux q related to the profile measured in random test: (a) CA_1, (b) CA_2, (c) CE_1 and (d) CE_2.

Moreover, the spreading around the carrier wave seen for RE_2, and probably due to the 2nd harmonic disturbance, leads to more homogeneous erosion phenomena compared to RE_1, where the formation of a well visible bar is recognizable. Final profiles and net sediment transport were consistent with these initial estimates [48]. Despite the fact that RE_1, RE_2, CE_1 and CE_2 have identical spectral energy, their local effect on beach profile can be significantly different due the presence of LFWs effectively influencing the spectra. The greater concentration of power at certain frequencies due to larger wave grouping could promote a stronger influence of LF motions in the SZ, in particular for two reasons:

1. specific eigenmode of the wave flume (generated seiches) induces spreading or downshift of carrier wave frequency, as foreseen;
2. grouping of short waves in the inner surf zone could directly induce low-frequency oscillations of the shoreline.

As termed by Russell [61] and Smith and Mocke [62], LFWs are powerful agents of sediment transport as they remove large amounts of the sediment which is put into suspensions by the short (wind) waves.

5.1. Influence on Morphodynamic

Figures 11 and 12 summarize the net sediment volume variation, ΔV_{SZ} , in the SZ (here approximated as the emerged beach) between the test start and end. These were obtained using the changes in bed elevation between profiles, above $z = 0$. Focus on the emerged SZ, during the analyzed first step of experiments, all wave conditions lead to a landward net sediment transport, except cases RE_2 and CE_1. For these wave conditions, the energy density associated with the second harmonic has been found about ten times the power level of the first mode, increasing the disturbance effect of the 2nd harmonic itself. Although erosive random waves have the same wave height and mean period, their morphological effect is quite different. It is noted that the grouping factor could promote the presence of multiple low-frequency motions responsible of nonlinear interactions. For this reason, there is a significant contribution that determines the evolution of surface changes. Unfortunately, the case CE_1 formed part of the tests that developed lateral cross-flume asymmetry; this does not significantly alter the wave height on WG 5, but the profile correction may not be sufficient for SZ sediment volume here computed. Hence, results for that case are not reported in Figure 12.

It is important to note as case CE_2 shows a positive net sand volume variation in the emerged SZ greater than accretive cases. Such conditions, however, are not in contrast with the typical erosion pattern along the whole profile (see [20]) of case CE_2. The reason for such strong “apparent” accretive behaviour in the SZ should be addressed to the initial beach profiles that, in such experiments, were usually the same or very similar for all wave conditions. Hence, in erosive conditions the beach is moving more rapidly toward an approximate equilibrium profile, and the mean beachface slope change induced by erosion of sediment provide some local deposition/positive slope change.

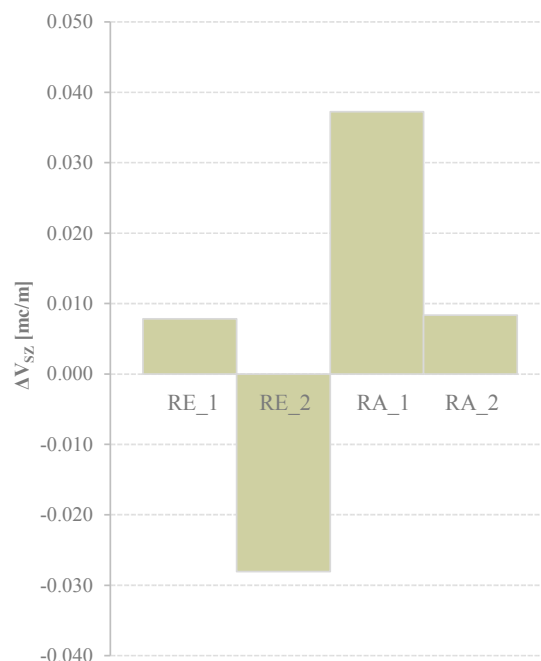


Figure 11. Net sand volume variation in the emerged swash zone (water depth > 0) after 24 min of wave generation: positive values represent accretion or landward transport; negative values represent erosion or seaward transport, for random tests.

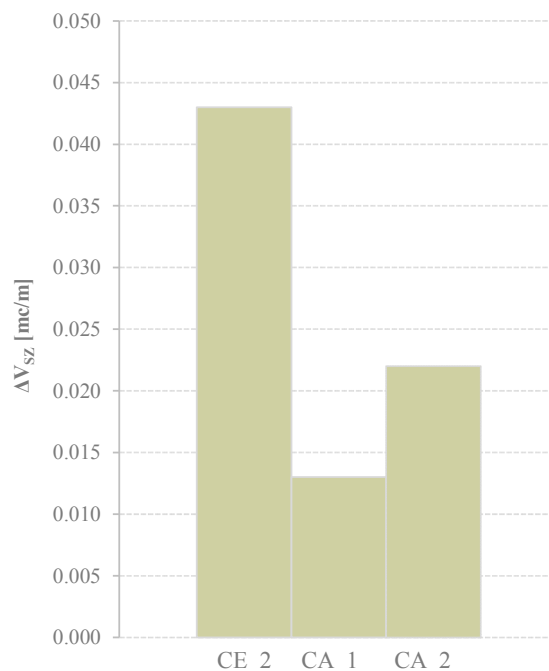


Figure 12. Net sand volume variation in the emerged swash zone (water depth > 0) after 24 min of wave generation: positive values represent accretion or landward transport for combination tests.

5.2. Influence on Swash Hydrodynamics

A tentative correlation between detected LFWs and runup is reported in the following. The measurements of runup have been conducted by a PC-based acquisition of digital camera records. Data processing has been carried out by using Image Processing Toolbox™ in MATLAB™ (version 2017, Natick, MA, USA). The camera was mounted on the profiler's carriage at rest, close to the board of the beach and focused on the wave flume. The camera was calibrated every time that it was removed from the waterproof housing (i.e., when profiler was operating). The calibration procedure consists of determining the relative position of a minimum of four points ("targets") in order to find the initial location and orientation of the camera relative to the calibration frame, as described by [63–67]. Since the position of instruments (captured in the video records) was known, eight "target" points were used, enhancing the quality of analysis. Then, the process was automatically completed by the definition of all remaining pixel position on the frame. In particular, the relative position of runup (as separation between dry and wet zones) was identified.

Runup measurements took place within the first three minutes of each step in order to identify the role of spectral wave components and wave grouping on runup, starting from the same underlying beach conditions.

The good agreements between runup values from video analysis and the ones derived by the extrapolation of measurements from micro-acoustic wave gauges (which only provide the height of the swash lens) on some uprush/backwash cycle give confidence in the technique.

The maximum runup measured are reported in Table 10. Looking at the table, some preliminary considerations can be drawn:

- "accretive" conditions do not necessarily involve smaller runup;
- despite comparable energy levels, random waves give a runup twice higher than combination cases;
- the higher the grouping factor the higher the maximum runup.

Hence, the data demonstrate that increasing differences in the spectral wave components through perturbations of monochromatic waves with long waves or increasing the grouping factor in random waves promotes the enhancement of wave run up, except for case R_E2.

Table 10. Maximum runup measured within the first three min of each step.

Test	Measured (m)	Test	Measured (m)
R_E1	0.36	R_A1	0.30
R_E2	0.41	R_A2	0.37
C_E1	0.16	C_A1	0.18
C_E2	0.12	C_A2	0.23

6. Conclusions

Experimental data from CIEM large-scale wave flume were specifically used to investigate low frequencies generated by random and combination waves in accretive and erosive conditions.

By examining the spectral distribution of wave power, a secondary downshifted peak around the carrier wave has been noted for conditions (both erosive and accretive) with higher grouping factor. This spreading takes the form of a second downshifted peak of about ± 0.045 Hz, an amount approximately equal to the second harmonic. Through the Eigen analysis it has been possible to estimate the periods of the dominant seiches in the wave flume and detect the low frequencies for combination and random waves. Then, comparing measured and calculated Eigenvalues for a rectangular wave flume, a good correspondence for the first and second harmonic has been found. Consequently, the wave flume-generated nature of first and second harmonic has been definitively clarified.

During the analyzed first step of experiment, all wave conditions lead to a landward net sediment transport in the swash zone, except cases RE_2 and CE_1 (Figures 11 and 12). For these wave conditions, the energy density associated to the second harmonic has been found to be about ten times the power level of the first mode, increasing the disturbance effect of the 2nd harmonic itself. However, case CE_1 contained errors due to cross-flume asymmetry of the evolving beach profile. Direct comparison of this test with the other erosive conditions is, therefore, not possible.

In the case of the erosive random waves, the presence of multiple low-frequency motions is responsible for nonlinear interactions, promoted by the grouping factor. Therefore, LFWs contribute significantly to the evolution of surface displacements.

The hydro-morphodynamic effects of the LFWs have been assessed by a volume flux Eigenmode analysis.

A clear opposite pattern of volume flux Eigenmode depending on accretive or erosive behaviour of wave conditions has been detected, except for the test CE_2. Despite the fact that the final profile and net sediment transport are consistent with the erosive trend, this test has shown an unexpected response on swash zone hydro-morphodynamics; the behavior is closer to a typical accretion wave condition.

A pattern of energy exchange between modes has been identified for all the tests in proximity of the breaking zone.

Results observed for swash zone volume variations measured during the first step (i.e., in comparable morphodynamic initial condition between tests) could be directly addressed to resonance phenomena in the wave flume. They may be also representative of real resonant conditions which could be generated landward of a submerged breakwater or in a natural enclosed basin (e.g. pocket beach with large secondary bar).

Clearly, the magnitude of net sediment volume in the swash zone suggests that low frequency motions could have a significant influence only on generation/development of secondary bedforms. In fact, morphodynamic effects of the seiches seem recognizable and significant only at a certain scale of observation. On the other hand, hydrodynamic influence on runup is more evident, but further analysis is required.

Future works will consider the last steps of each test, in order to investigate the low frequencies when affected by morphodynamic effects and vice versa (e.g. bedforms migration).

Acknowledgments: This work was supported by the European Community's Sixth Framework Programme through the grant to the budget of the Integrated Infrastructure Initiative HYDRALAB III within the Transnational Access Activities, Contract No. 022441. Special thanks go to Prof. James Kirby (University of Delaware) and Iván Cáceres (Universitat Politècnica de Catalunya) for their help to analyze data.

Author Contributions: Pasquale Contestabile performed the laboratory experiments; Luigia Riefolo conceived the analysis tools; Luigia Riefolo, Fabio Dentale and Guido Benassai contributed to analysis of the data; Luigia Riefolo and Pasquale Contestabile wrote the paper; Fabio Dentale and Guido Benassai revised the paper draft; Luigia Riefolo updated the paper according to their review.

Conflicts of Interest: The authors declare no conflict of interest.

References

1. Budillon, F.; Vicinanza, D.; Ferrante, V.; Iorio, M. Sediment transport and deposition during extreme sea storm events at the Salerno Bay (Tyrrhenian Sea): Comparison of field data with numerical model results. *Nat. Hazards Earth Syst. Sci.* **2006**, *6*, 839–852. [[CrossRef](#)]
2. Brocchini, M.; Bellotti, G. Integral flow properties of the swash zone and averaging. Part 2. Shoreline boundary conditions for wave-averaged models. *Int. J. Fluid Mech. Res.* **2002**, *458*, 269–281. [[CrossRef](#)]
3. Oltman-Shay, J.; Howd, P.A.; Birkemeier, W.A. Shear instabilities of the mean longshore current: 2. Field observations. *J. Geophys. Res. Oceans* **1989**, *94*, 18031–18042. [[CrossRef](#)]
4. Miles, J.R.; Russell, P.E.; Ruessink, B.G.; Huntley, D.A. Field observations of the effect of shear waves on sediment suspension and transport. *Cont. Shelf Res.* **2002**, *22*, 657–681. [[CrossRef](#)]
5. Watson, G.; Barnes, T.C.D.; Peregrine, D.H. The generation of low-frequency waves by a single wave group incident on a beach. *Coast. Eng.* **1994**, *1995*, 776–790.
6. Mase, H. Frequency down-shift on swash oscillations compared to incident waves. *J. Hydraul. Res.* **1995**, *33*, 397–411. [[CrossRef](#)]
7. Suhayda, J.N. Standing waves on beaches. *J. Geophys. Res.* **1974**, *79*, 3065–3071. [[CrossRef](#)]
8. Huntley, D.A.; Guza, R.T.; Bowen, A.J. A universal form for shoreline run-up spectra. *J. Geophys. Res.* **1977**, *82*, 2577–2581. [[CrossRef](#)]
9. Guza, R.T.; Thornton, E.B. Swash oscillations on a natural beach. *J. Geophys. Res.* **1982**, *87*, 483–491. [[CrossRef](#)]
10. Holland, K.T.; Raubenheimer, B.; Guza, R.T.; Holman, R.A. Runup kinematics on a natural beach. *J. Geophys. Res.* **1995**, *100*, 4985–4993. [[CrossRef](#)]
11. Raubenheimer, B.; Guza, R.T. Observations and predictions of run-up. *J. Geophys. Res.* **1996**, *101*, 25575–25587. [[CrossRef](#)]
12. Van Dongeren, A.; Lowe, R.; Pomeroy, A.; Trang, D.; Roelvink, D.; Symonds, G.; Ranasinghe, R. Numerical modeling of dynamics over a fringing coral reef. *Coast. Eng.* **2013**, *73*, 178–190. [[CrossRef](#)]
13. Ruju, A.; Lara, J.L.; Losada, I.J. Numerical analysis of run-up oscillations under dissipative conditions. *Coast. Eng.* **2014**, *86*, 45–56. [[CrossRef](#)]
14. De Bakker, A.T.M.; Tissier, M.F.S.; Ruessink, B.G. Beach steepness effects on nonlinear infragravity-wave interactions: A numerical study. *J. Geophys. Res. Oceans* **2015**, *121*. [[CrossRef](#)]
15. Bowen, A.J.; Inman, D.L. Edge waves and crescentic bars. *J. Geophys. Res.* **1971**, *76*, 8662–8671. [[CrossRef](#)]
16. Huntley, D.A.; Guza, R.T.; Thornton, E.B. Field observations of surf beat: 1. Progressive edge waves. *J. Geophys. Res.* **1981**, *86*, 6451–6466. [[CrossRef](#)]
17. Guza, R.T.; Thornton, E. Observations of surf beat. *J. Geophys. Res.* **1985**, *90*, 3161–3172. [[CrossRef](#)]
18. Oltman-Shay, J.; Guza, R.T. Infragravity edge wave observations on two California beaches. *J. Phys. Oceanogr.* **1987**, *17*, 644–663. [[CrossRef](#)]
19. Holland, K.T.; Holman, R.A. Wavenumber-frequency structure of infragravity swash motions. *J. Geophys. Res.* **1999**, *104*, 13479–13488. [[CrossRef](#)]
20. Baldock, T.E.; Alsina, J.; Cáceres, I.; Vicinanza, D.; Contestabile, P.; Power, H.; Sanchez-Arcilla, A. Large-scale experiments on beach profile evolution and surf and swash zone sediment transport induced by long waves, wave groups and random waves. *Coast. Eng.* **2011**, *58*, 214–227. [[CrossRef](#)]

21. Watson, G.; Peregrine, D.H.; Toro, E.F. Numerical solution of the shallow-water equations on a beach using the weighted average flux method. In Proceedings of the First European Computational Fluid Dynamics Conference, Brussels, Belgium, 7–11 September 1992; Volume 1, pp. 495–502.
22. Baldock, T.E.; Holmes, P.; Horn, D.P. Low frequency swash motion induced by wave grouping. *Coast. Eng.* **1997**, *32*, 197–222. [[CrossRef](#)]
23. Brocchini, M. Eulerian and Lagrangian aspects of the longshore drift in the surf and swash zones. *J. Geophys. Res. Oceans* **1997**, *102*, 23155–23168. [[CrossRef](#)]
24. Masselink, G.; Puleo, J.A. Swash-zone morphodynamics. *Cont. Shelf Res.* **2006**, *26*, 661–680. [[CrossRef](#)]
25. Brocchini, M.; Baldock, T.E. Recent advances in modeling swash zone dynamics: Influence of surf-swash interaction on nearshore hydrodynamics and morphodynamics. *Rev. Geophys.* **2008**, *46*. [[CrossRef](#)]
26. Horn, D.P.; Baldock, T.E.; Li, L. The influence of groundwater on profile evolution of fine and coarse sand beaches. In Proceedings of the Sixth International Symposium on Coastal Engineering and Science of Coastal Sediment Process, New Orleans, LA, USA, 13–17 May 2007.
27. Ciavola, P.; Vicinanza, D.; Fontana, E. Beach drainage as a form of shoreline stabilization: case studies in Italy. In Proceedings of the 31st International Conference on Coastal Engineering, Hamburg, Germany, 31 August–5 September 2008.
28. Ciavola, P.; Vicinanza, D.; Aristodemo, F.; Contestabile, P. Large-scale morphodynamic experiments on a Beach Drainage System. *J. Hydraul. Res.* **2011**, *49*, 523–528. [[CrossRef](#)]
29. Damiani, L.; Aristodemo, F.; Saponieri, A.; Verbeni, B.; Veltri, P.; Vicinanza, D. Full-scale experiments on a beach drainage system: Hydrodynamic effects inside beach. *J. Hydraul. Res.* **2011**, *49*, 44–54. [[CrossRef](#)]
30. Contestabile, P.; Aristodemo, F.; Vicinanza, D.; Ciavola, P. Laboratory study on a beach drainage system. *Coast. Eng.* **2012**, *66*, 50–64. [[CrossRef](#)]
31. Ciavola, P.; Contestabile, P.; Aristodemo, F.; Vicinanza, D. Beach sediment mixing under drained and undrained conditions. *J. Coast. Res.* **2013**, *65*, 1503–1508. [[CrossRef](#)]
32. Mansard, E.P.D.; Sand, S.E. A Comparative Evaluation of Wave Grouping Measures. In Proceedings of the 24th International Conference on Coastal Engineering, Kobe, Japan, 23–28 October 1994.
33. Merrick, C.; Haller, C.; Dalrymple, R.A. Looking for Wave Groups in the Surf Zone. In Proceedings of the International Conference on Coastal Research in Terms of Large Scale Experiments, Gdansk, Poland, 4–8 September 1995; pp. 81–92.
34. Baldock, T.E.; Manoonvoravong, P.; Pham, K.S. Sediment transport and beach morphodynamics induced by free long waves, bound long waves and wave groups. *Coast. Eng.* **2010**, *57*, 898–916. [[CrossRef](#)]
35. Dally, W.R. Long Wave Effects in Laboratory Studies of Cross-Shore Transport. 1991. Available online: <http://cedb.asce.org/CEDBsearch/record.jsp?dockey=0071660> (accessed on 21 February 2018).
36. Baldock, T.E.; Huntley, D.A. Long-Wave Forcing by the Breaking of Random Gravity Waves on a Beach. *Philos. Trans. R. Soc. Lond. Ser. A* **2002**, *458*, 2177–2201. [[CrossRef](#)]
37. Hydrolab III. EU Integrated Infrastructure Initiative, SUSCO Swash Zone Response under Grouping Storm Conditions. Available online: <http://hydralab.eu/research--results/ta-projects/project/97/> (accessed on 21 February 2018).
38. Haller, M.C.; Dalrymple, R.A. Rip current instabilities. *J. Fluid Mech.* **2001**, *433*, 161–192. [[CrossRef](#)]
39. Sorensen, R.M. *Basic Wave Mechanics: For Coastal and Ocean Engineers*; John Wiley & Sons, Inc.: Hoboken, NJ, USA, 1993.
40. Bellotti, G.; Archetti, R.; Brocchini, M. Experimental validation of mean swash zone boundary conditions. *J. Geophys. Res.* **2003**, *108*, 3250. [[CrossRef](#)]
41. Young, I. Observations of triad coupling of finite depth wind waves. *Coast. Eng.* **1998**, *33*, 137–154. [[CrossRef](#)]
42. Losada, M.A.; Roldan, A.J.; Dalrymple, R.A. Eigenfunction analysis of water wave propagation down a wave flume. *J. Hydraul. Res.* **1994**, *32*, 371–385. [[CrossRef](#)]
43. Van Dongeren, A.; Battjes, J.; Janssen, T.; van Noorloos, J.; Steenhauer, K.; Steenbergen, G.; Reniers, A. Shoaling and shoreline dissipation of low-frequency waves. *J. Geophys. Res.* **2007**, *112*. [[CrossRef](#)]
44. Patel, M.H.; Ionnaou, P.A. Comparative Performance Study of Paddle- and Wedge-Type Wave Generators. *J. Hydronaut.* **1980**, *14*, 5–9. [[CrossRef](#)]

45. Riefolo, L.; Contestabile, P.; Ferrante, V.; Azzellino, A.; Centurioni, L.; Vicinanza, D. The role of spectral wave components, bandwidth and wave grouping on runup: Preliminary results from large-scale experiments. In Proceedings of the 5th International Conference on the Application of Physical Modelling to Port and Coastal Protection Coastlab14, Varna, Bulgaria, 29 September–2 October 2014.
46. Moreno, L.J. Perfil de Playas Sustentadas: Estudio Hidrodinámico y Experimental. Directrices de Diseño. Ph.D. Thesis, Technical University of Madrid, Madrid, Spain, 2016.
47. Dean, R.G. Heuristic models of sand transport in the surf zone. In Proceedings of the First Australian Conference on Coastal Engineering, Sydney, Australia, 14–17 May 1973.
48. Vicinanza, D.; Baldock, T.E.; Contestabile, P.; Alsina, J.; Cáceres, I.; Brocchini, M.; Conley, D.; Andersen, T.L.; Frigaard, P.; Ciavola, P. Swash Zone Response under Grouping Storm Conditions. *J. Hydraul. Res.* **2011**, *4*, 55–63. [[CrossRef](#)]
49. Wright, L.D.; Short, A.D. Morphodynamic variability of surf zones and beaches: A synthesis. *Mar. Geol.* **1984**, *56*, 93–118. [[CrossRef](#)]
50. Aalborg University. Software for Wave Laboratories. Available online: <http://hydrosoft.civil.aau.dk/AwaSys/> (accessed on 17 February 2018).
51. Hald, T. *Wave Group Analysis by Means of the Hilbert Transform Technique*; Aalborg University: Aalborg, Denmark, 1995.
52. Munoz-Perez, J.J.; Caballero, I.; Tejedor, B.; Gomez-Pina, G. Reversal in longshore sediment transport without variations in wave power direction. *J. Coast. Res.* **2010**, 780–786. [[CrossRef](#)]
53. Molloy, E. Seiching in Cockburn Sound. Master's Thesis, University of Western Australia, Crawley, WA, Australia, November 2001.
54. Rabinovich, A.B. Seiches and Harbor Oscillations. In *Handbook of Coastal and Ocean Engineering*; Kim, Y.C., Ed.; World Scientific: Singapore, 2009.
55. Merian, J.R. Ueber die Bewegung tropfbarer Flüssigkeiten in Gefässen [On the Motion of Drippable Liquids in Containers]. Master's Thesis, Göttingen University, Göttingen, Germany, 1828. (In German)
56. Wilson, B. Seiches. In *Advances in Hydrosiences*; Academic Press: Urbana, IL, USA, 1972; Volume 8, pp. 1–94.
57. Kirby, J.T.; Özkan-Haller, H.T.; Haller, M.C. Seiching in a large wave flume. In Proceedings of the 30th International Conference on Coastal Engineering, San Diego, CA, USA, 3–8 September 2006.
58. Cáceres, I.; Alsina, J.M. Suspended sediment transport and beach dynamics induced by monochromatic conditions, long waves and wave groups. *Coast. Eng.* **2016**, *108*, 36–55. [[CrossRef](#)]
59. Svendsen, I.A. Mass flux and undertow in a surf zone. *Coast. Eng.* **1984**, *8*, 347–365. [[CrossRef](#)]
60. Riefolo, L.; Azzellino, A.; Ferrante, V.; Contestabile, P.; Vicinanza, D. Wave flume-generated seiching analysis. In Proceedings of the Twenty-fifth International Ocean and Polar Engineering Conference, Kona, Big Island, HI, USA, 21–26 June 2015.
61. Russell, P.E. Mechanisms for beach erosion during storms. *Cont. Shelf Res.* **1993**, *13*, 1243–1265. [[CrossRef](#)]
62. Smith, G.G.; Mocke, G.P. Interaction between breaking/broken waves and infragravity-scale phenomena to control sediment suspension transport in the surf zone. *Mar. Geol.* **2002**, *187*, 329–345. [[CrossRef](#)]
63. Benassai, G.; Aucelli, P.; Budillon, G.; De Stefano, M.; Di Luccio, D.; Di Paola, G.; Montella, R.; Mucerino, L.; Sica, M.; Pennetta, M. Rip current evidence by hydrodynamic simulations, bathymetric surveys and UAV observation. *Nat. Hazards Earth Syst. Sci.* **2017**, *17*, 1493. [[CrossRef](#)]
64. Nunziata, F.; Buono, A.; Migliaccio, M.; Benassai, G. Dual-polarimetric C- and X-band SAR data for coastline extraction. *IEEE J. Sel. Top. Appl. Earth Obs. Remote Sens.* **2016**, *9*, 4921–4928. [[CrossRef](#)]
65. Nunziata, F.; Migliaccio, M.; Li, X.; Ding, X. Coastline extraction using dual-polarimetric COSMO-SkyMed PingPong mode SAR data. *IEEE Geosci. Remote Sens. Lett.* **2014**, *11*, 104–108. [[CrossRef](#)]
66. Nunziata, F.; Buono, A.; Migliaccio, M.; Benassai, G. An Effective Method to Extract Coastline from Dual-Polarimetric C- and X-Band SAR Measurements. Available online: http://lps16.esa.int/page_paper0891.php (accessed on 21 February 2018).
67. Benassai, G.; Migliaccio, M.; Montuori, A. Sea wave numerical simulations with COSMO-SkyMed© SAR data. *J. Coast. Res.* **2013**, *65*, 660–665. [[CrossRef](#)]

